ICAS-88-1.11.4

# COMPUTATIONAL DESIGN AND EFFICIENCY OPTIMIZATION OF AGRICULTURAL AIRPLANES

Rolf Staufenbiel (1), Thomas Scherer (1), Istvan Steiger (2)

(1) Technical University of Aachen, FRG
(2) Technical University of Budapest, Hungary

## Abstract

The operational efficiency of agricultural aircrafts depend mainly on the uniformity of the spray distribution and the width of the spray corridor. A simulation program has been developed for optimizing the parameters of the spraying system and the configuration of agricultural airplanes. This simulation gives higher accuracy in calculated spraying distribution, as well as other improvements when compared to existing methods. In particular, new techniques for describing the roll-up process of the wing wake and the flow characteristics of the propeller slipstream were introduced. In addition, a new statistical method for describing the influence of wind fields and turbulence has been used.

Using this simulation program, improvements in spray efficiency resulting from various modifications of an existing aircraft have been evaluated. By installing winglets, in addition to a favorable influence on the aircraft performance, spray efficiency can be improved. This winglet configuration has been investigated, in combination with optimized spray nozzle arrangements, in flight tests. These tests were performed in Hungary using an agricultural airplane of PZL M-18 DROMADER type in cooperation with the Technical University of Budapest. In general, a good agreement between flight tests and simulation results was found.

## I. Introduction

Airplanes play an important part in the cultivation of agricultural and forestry crops. About 5% of the entire world's agricultural area and 15% of the US area are sprayed by aircraft, mostly with toxic chemicals.

In usual applications liquid spray pesticides are dispersed at a rate that covers the target area with a "toxic carpet", which may have about a hundred times overkill capability. Insofar, as ecological impact, insecticide resistance and environmental pollution have been a growing concern, new methods of spray application had to be developed during the last decade[1-5].

Most chemicals need to get into direct contact with the insects. Hence the minimum number of droplets per area is determined by the dimensions of the target insect. Normal spray droplets have a size of 200 to 300 micrometer and contain 100 or 1000 lethal doses for the target insect. In principle the droplet size could be decreased down to about 10 micrometers without changing the mortality of the spray. However, since droplets of this size are easily dispersed by wind, their deposition cannot be readily controlled. For practical use a high uniformity of the spray deposition combined with maximum width of the spray corridor and minimal wind drift is needed.

Using a computer simulation, the economical and ecological aspects of aerial spraying can be optimized by improving the aerodynamic configuration of agricultural aircraft and the arrangement of the spraying equipment. Although a lot of full scale and modeled experiments concerning the distribution of aerial sprays have been performed, there is still a demand for more powerful computer simulations.

The basic works of W.Reed[6-7] and Trayford and Welch[8-9] are the only simulations known up to now. They are able to compute droplet trajectories influenced by a simplified wake of a low flying aircraft. The basic factors which influence droplet motion such as tip vortices, ground effect, propeller swirl, cross-wind are considered, and the resulting spray distributions estimated. For the investigations of the deposition of small droplets the models used in these papers do not seem to be sufficient.

The present paper describes a simulation in which the most important influences on the spray deposition are reviewed and modeled. In particular, refinements are introduced for simulating

- the roll-up of the wing wake,
- the propeller slipstream,
- influences of cross-wind and air turbulence.

Using this simulation program, improvements of the spraying quality by modifying the wing configuration have been investigated. In particular the effects of winglets and changes in the spray nozzle installation have been investigated.

A contract of cooperation with the Hungarian academy of sciences made it possible to verify the simulation results in flight tests conducted in Budapest and Nyiregyhza using a PZL M-18 DROMADER (Fig. 1).

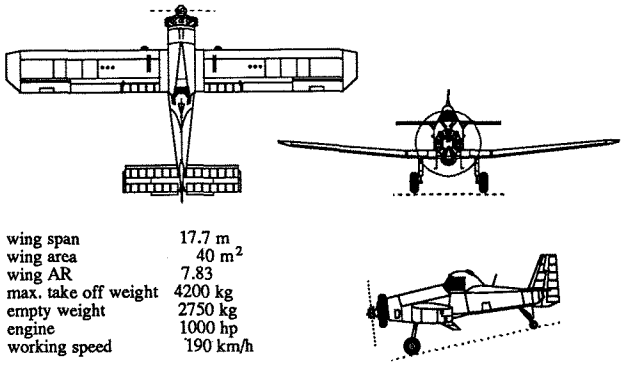


Figure 1. Agricultural aircraft used in the investigation, PZL M-18 Dromader

## II. The Simulation System

### General Description of the Simulation Procedure

Several steps are required to compute the spray distribution.

- First, the aerodynamic characteristics of the airplane must be determined for a given spray mission. The distribution of circulation for the wing-body configuration, which determines the aircraft wake, is calculated using a standard vortex-lattice program. The propeller slipstream and interference with the wing is included.

- In the next step, the roll-up of the vortex sheet, shed from the trailing edge of the wing, is computed. The sheet is represented by discrete vortex lines and the roll-up is calculated by a three-dimensional near-field solution together with a two-dimensional far-field method.

- The trajectories of single droplets influenced by this flow field are then computed. The droplet motion is determined under consideration of the flow fields of the wake and the cross-wind, taking into account droplet evaporation. This part requires the major portion of the computational time.

- The ground deposition pattern of a single spray nozzle is computed by means of a statistical assessment from the data of all droplets emitted at the same wing span position. The assessment includes cross-wind, atmospheric turbulence and the spray nozzle characteristics as droplet spectra, spray-cone angles, spray duct pressure etc.

- The spray distribution for a chosen arrangement of the spray nozzle on the spray boom can now be evaluated by superimposing the distributions calculated for the single nozzles.

- If distributions for a number of nozzle positions have been calculated, an optimal spray nozzle arrangement can be found by an evolutionary strategy that minimizes the statistical deviation from a desired uniform spray distribution.

As this sequence of calculations has to be repeated for any new aerodynamic configuration of the airplane, the influences that have a major effect on the spray quality should be studied carefully before a modification of the airplane is proposed.

The following sections discuss each part of the simulation and present basic results.

## III. Airplane Aerodynamics

As disturbances caused by the aircraft have a fundamental influence on the droplet motion, the wake of wing, fuselage and propeller has to be modeled as accurately as possible. The particular aircraft considered here is the Polish PZL M-18 DROMADER.

For the calculation of the flow field around the wing and body configurations a NASA vortex-lattice program[10] has been used, which is also able to include the ground effect. The complex shape of the DROMADER fuselage was simplified by modeling it by a short cylinder with spherical front and end caps. The surface of the wing-body configuration was discretizised into 150 panels, arranged on the wing, and 90 panels on the body. The panels on the wing were distributed in three chordwise rows of 50 spanwise panels each. For the winglet configuration, the wing panel number was increased to 210. The accuracy achieved by this panel arrangement proved to be sufficiently high.

Because the vortex-lattice program is not able to treat directly the propeller slipstream as a non-uniform flow, the propeller flow was modeled in the following way. The propeller slipstream induces large velocities on the wing. The axial velocity increases the dynamic pressure of the wing, while the propeller swirl changes the angle of attack. Both effects lead to a strong modification of the circulation distribution. This is included in the computation using an additional twist on those wing sections which are located in the slipstream.

The calculation of the axial and tangential velocities in the propeller slipstream is performed with a free wake analysis method, proposed by Müller[11], which was originally developed for helicopter rotors. The rotor geometry, rotor speed and flight velocity are inputs for this method. The circulation on the propeller blades and the velocity components in the propeller wake are the outputs (Fig. 2). In addition, the thrust of the propeller and the required power are evaluated. These can be used for evaluating the accuracy of the method. The profile drag of the blades is not included because their contribution to the propeller swirl is less than 5% for lower blade tip velocities ($M \leq 0.6$).

The computations were done for a free propeller, where the propeller disk is considered to be a ring that fits around the fuselage.

The spanwise variation in circulation that results from the vortex-lattice computation as well as the strength of the trailing vortex sheet are shown in Fig. 3. The influence of the fuselage is concentrated near the plane of symmetry. The propeller swirl generates a strong vortex shed from the inner part of the left wing where the propeller flow is directed upwards. The bound and trailing vortices resulting from this computation are the inputs to the three- and two-dimensional roll-up programs, discussed in the next section.

Besides the original configuration of the DROMADER, an improved version has been investigated. The original wing was fitted with winglets optimized for minimum drag at high angles of attack. This design has the advantage of high aerody-

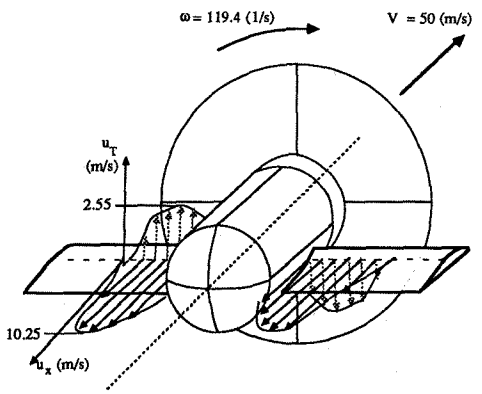


Figure 2. Velocity distribution in the propeller wake

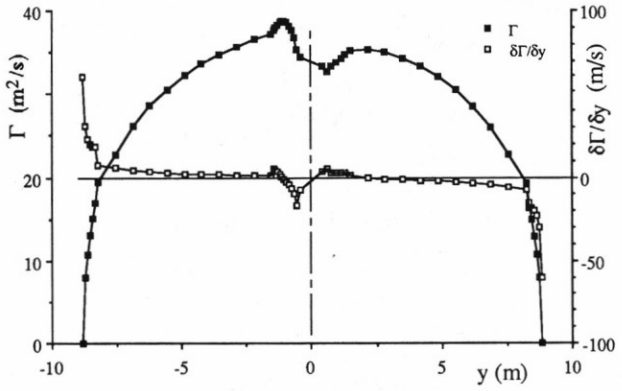


Figure 3. Distribution of circulation for the Dromader in spray flight ($C_L$=0.55, P=410 hp)

namic load on the winglet during the spray operation. This results in the tip vortex being located farther from the spray boom, with a reduced influence on the spray deposition.

The preliminary winglet geometry is obtained from a wing design code based on lifting line theory. The input data are the shape of the original wing, the dihedral angle and the span of the winglet. The design procedure determines an optimal distribution of winglet chord length (Fig. 4a). This procedure takes into account the fixed maximum value of the wing root bending moment, the yaw-induced rolling moment as well as the limit of the side-slip angle at which the flow on the winglet is still fully attached.

Wind-tunnel results have shown that the fairings between the main wing and the winglet have to be designed thoroughly to prevent boundary-layer separations. After finishing the optimization the geometry has been smoothed by hand to achieve a manufacturable winglet geometry (Fig. 4b).

The final step of the design uses a vortex-lattice method to adjust the twist distribution on the winglet (Fig. 4c). The resulting winglet (Fig. 4d and 5) gives some reduction in drag during maneuver and climb as well as a considerable tip-vortex displacement during spray operation.

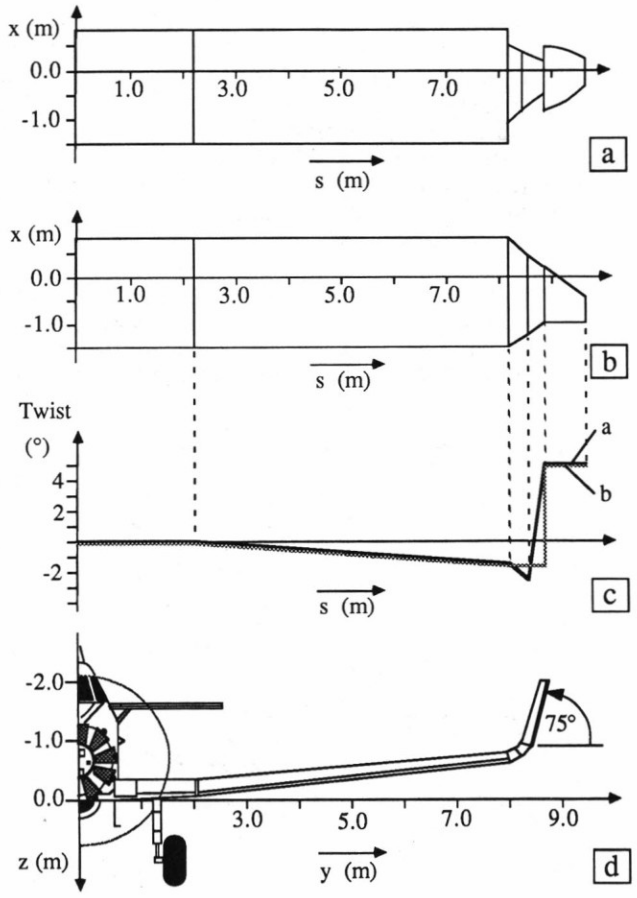


Figure 4 Steps of winglet design using a drag minimization code

## IV. Modeling of the Vortex Roll-up

To ensure a sufficiently accurate computation of droplet trajectories, a realistic modeling of the roll-up of the vortex sheet is of fundamental importance. The following model is used in the simulation program.

Within ten chord lengths behind the wing, the roll-up is computed by a three-dimensional free wake model. Then, the calculation switches over to a two-dimensional time-dependent code using a modified point vortex method. This point vortex method gives quite accurate results for the flow field far behind the wing without the excessive computer time needed for the free wake model.

The free wake model[12] starts from a straight vortex sheet shed at the trailing edge of the wing. The vortex filaments, which form the sheet, are shed from the borders of the panels used in the vortex-lattice program. Each vortex filament consists of twenty straight segments, which are convected parallel to the inflow, all of them carrying a control point. The shape of the wake is determined by an iteration procedure. In every pass, the new positions of the vortex segments are determined rowwise in span direction starting at the trailing edge of the wing. Each segment of a row is aligned to the direction of the flow vector at its control point. This scheme is repeated until every row of vortex segments filament has been directed. Then, the whole procedure is repeated until the shape of the vortex sheet becomes stable (Fig. 6). Usually, three iterations are sufficient.

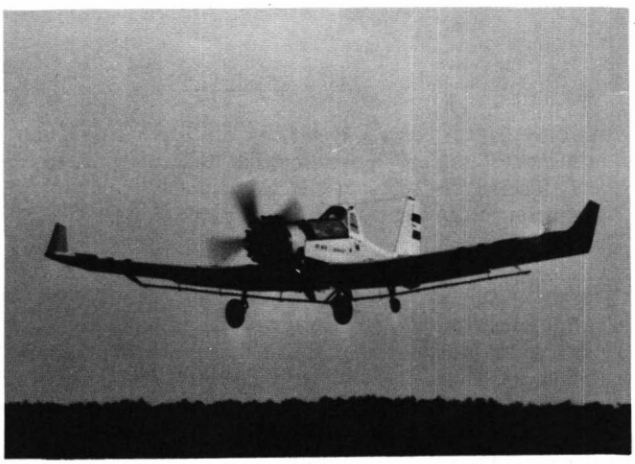

Figure 5. PZL M-18 fitted with winglets

The computation of the flow vectors is done by a superposition of the inflow and the velocities induced by bound vortices and vortex segments in the wake. Downstream of the last vortex segment a line vortex of infinite length, running parallel to the x-axis, is assumed. The induced velocities are computed by the Biot-Savart law with the assumption that the vortex filaments have a finite core radius. The vortex core is described by a Rankine vortex model. The ground effect is considered by the mirror image method.

The propeller swirl and slipstream is concentrated in a tube having the diameter of the propeller and being oriented parallel to the inflow direction. The widening of the flow tube is neglected. The distribution of the axial and tangential velocity in this tube is as illustrated in Fig. 2. The propeller flow field decreases quickly due to turbulent mixing. Instead of using an artificial decay model the direct influence of the propeller is limited to the short part of the vortex sheet that is described by the free wake model.

The two-dimensional roll-up starts from the last cross-section of the free wake. The method used is a point vortex algorithm which is modified by a special way of vortex amalgamation technique to handle the problem of chaotic motion.

The roll-up process is computed over a length of 550 chords to ensure that the simulation can deal with longer lasting droplets. The vortex motion is determined by a Runge-Kutta integration scheme. The ground effect is considered again by the mirror image of the vortices filaments. The time step of the integration is controlled by an estimated local error. To ensure tolerable computation time, the minimum time step is limited.

The global accuracy of the roll-up can be checked by an evaluation of the vortex sheet energy e, which should be an invariant of the integration. The energy of a discrete vortex sheet can be determined by the Kirchhoff-Routh function[13]

$$e = \rho\,(-1/2\pi) \sum_{i=1}^{N-1} \sum_{j=i-1}^{N} \gamma_i \gamma_j \ln (r_{ij}/s) \qquad (1)$$

This value is determined at the beginning of the roll-up (at the trailing edge of the wing) and subsequently checked.

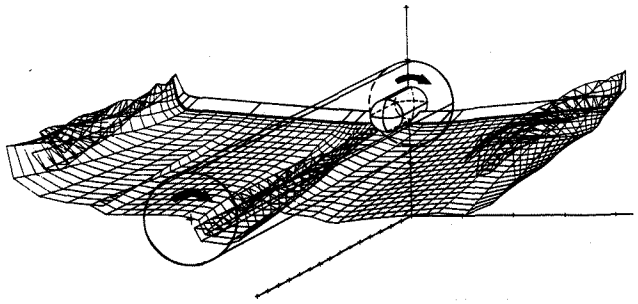

Figure 6. Wing-body-propeller configuration used in the simulation

Performing the integration rises a problem: As the point vortices, concentrated in the tip vortex core, are very close to each other, the control of the time step demands very small values for $\Delta t$ . Because $\Delta t$ is inversely proportional to $r^2$ (r distance between point vortices), values of $\Delta t$ on the order of $10^{-8}$ s are required for N=60 vortices and an elliptic wing loading. Even if the minimum value of $\Delta t$ is limited to $10^{-6}$, the computation still requires 20 hours on a Cyber 825-170. When a larger $\Delta t$ is enforced, the point vortices inside the tip vortex core increase their mutual distances rapidly until the radius of the vortex core is adapted to the chosen time step. During this short phase the vortical dispersion increases and, due to Equ. 1, the energy of the vortex is significantly diminished. Afterwards the changes of these parameters remain small. The violation of the energy conservation, not the chaotic motion in itself, is considered as a weak point of the standard point vortex method.

This problem can be resolved by using a special amalgamation procedure performed continuously during the roll-up. During the roll-up, the amalgamation gathers all point vortices of the sheet, which come to close to the core, into a single central vortex. The resulting rapid decrease of the vortex number during the roll-up makes it possible to use a smaller time step without raising the total demand of computation time.

The amalgamation procedure limits the spiral pattern of the vortex sheet outside the vortex core to one or two windings. The vortex core is represented by a single vortex placed in the center of the amalgamated point vortices. The structure of this core vortex is analytically described by the distribution of the vorticity and is modeled by a modified Lamb-model, structured by three free parameters (A, $R_k$, $\Lambda$):

$$\Gamma(r,t) = \Gamma_{core}(t)\left(A + (1-A)\,r/R_k\right)\left(1 - e^{-\Lambda r^2}\right) \qquad (2)$$

The free parameters are computed after every amalgamation step, resulting in a dynamically growing core vortex. During the amalgamation process, the values of two important characteristics of the vortex sheet change:

- The energy e (Eq. 1) and
- the vortical dispersion I.

This dispersion, introduced by BETZ[14], is given by

$$I = \int_0^{\infty} \frac{\partial \Gamma}{\partial r}\, r^2\, dr \qquad (3)$$

The energy should be kept constant throughout the roll-up process [15,16], while the vortical dispersion is invariant only for the roll-up of a half span vortex sheet. For a full span wake this value will increase slowly by about twenty percent. Therefore, I and e are considered to be suitable parameters to control the roll-up and amalgamation process.

Using the variation $\Delta e$ and $\Delta I$ during every amalgamation the parameters of the vortex model can be calculated. Two parameters of the vortex model, $\Lambda$ and $R_k$, are closely coupled to the values of energy and vortical dispersion. The third one, (A), is chosen from experiments and is set 0.68. After each amalga-

mation step new values of $\Lambda$ and $R_k$ are computed using the following formula:

$$\Lambda_{new} = \Lambda_{old} \exp\left(-\frac{8\pi \Delta e}{\rho \Gamma^2_{core/new}}\right) \qquad (4)$$

Using this value, $R_k$ can be determined for given values of $\Delta I$ and $I_{old}$ by

$$R_{K_{new}} = \sqrt{\frac{\frac{I_{old}+\Delta I}{\Gamma_{core/new}} - \frac{A}{\Lambda_{new}}}{1-A} - \frac{ERF\left(\sqrt{R_{K_{old}} \cdot \Lambda_{new}}\right)}{\sqrt{R_{K_{old}} \cdot \Lambda_{new}}}} \qquad (5)$$

The automatic adaptation of the vortex model ensures a good approximation of the structure and velocity distribution inside the tip vortex core during the entire roll-up [17,18].

An additional feature of the amalgamation is the possibility of correcting the loss of energy caused by the limitation of the integration time step. This is achieved by adapting the parameters of the vortex model at every amalgamation step directly to the initial value of the energy $e_0$ instead of to the momentary value, e.

The vortex sheet which results from this computation conserves the important invariants (Fig. 7) and needs only 1.4 hours to be computed. The velocity distribution of the roll-up

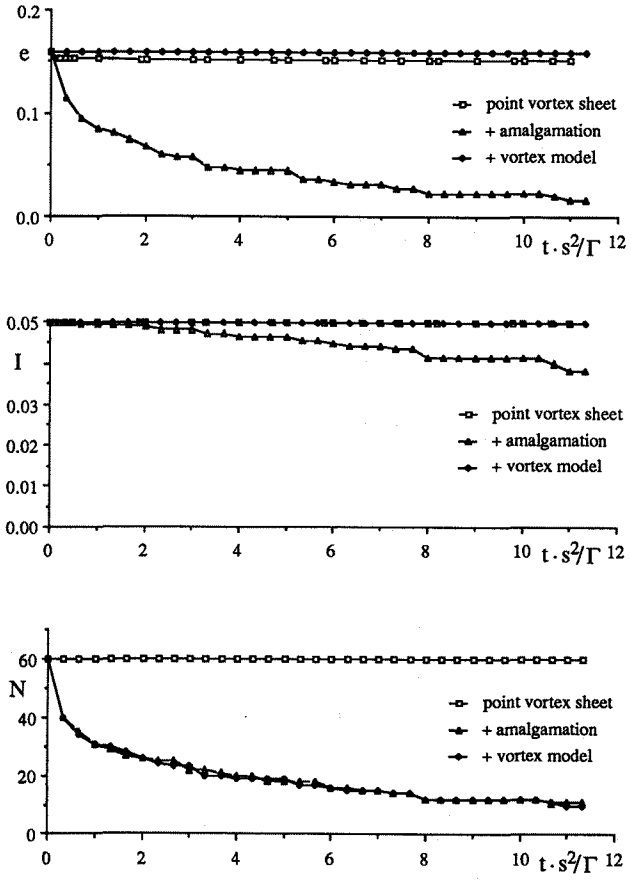


Figure 7. Development of vortex sheet energy, vortical dispersion and number of non-amalgamated vortices.

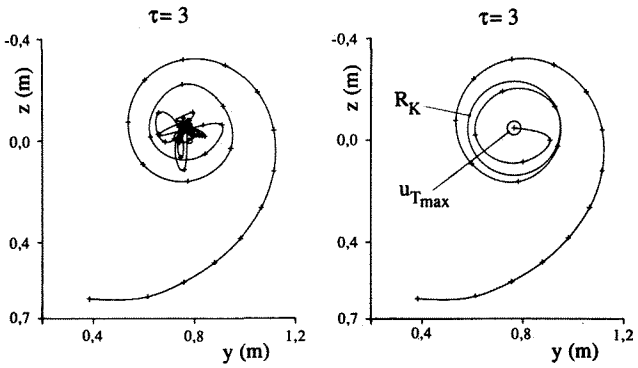


Figure 8: Rolled-up half span vortex sheet and amalgamated vortex sheet (in non-dimensional units)

tip-vortices shows good agreement with experiments and with numerical simulations using much more computer resources (Fig. 8). Additionally, the velocity distribution inside the core vortex is much smoother than found in the standard point vortex method (Fig. 9). This, and the rapidly decreasing number of point vortices required are advantages for the calculations of droplet trajectories to be described below.

## V. Computation of Droplet Motion

The motion of spray droplets will be considered in a space-fixed coordinate system. The droplet motion is determined by the aerodynamic drag and the gravity force

$$m_D(t)\ddot{\vec{x}} = m_D(t)\vec{g} + C_D\,(Re)\,A_D\,(t)\,\rho/2\,|\vec{U}_{rel}|\,\vec{U}_{rel} \qquad (6)$$

where $U_{rel}$ is the velocity of air relative to the moving droplet containing all influences of the wing wake and the propeller.

During the first few milliseconds of flight, the droplet is decelerated from the relatively high speed of the airplane to nearly the speed of the flow in the wake. During about 100 microseconds of this phase, very strong forces deform the droplet to a disk presenting a larger front area, which gives a further increase of the drag force. This process can continue until the droplet breaks up. Thus, this short phase is important for the formation of the spray cloud. This break-up process has not been explicitly considered in this simulation. It has been accounted for by using measured values for the shape of the spray cloud and the spectra of droplet sizes behind the emitting nozzle, after the break-up.

As the region of droplet deformation and break-up is smaller than 5 cm, the computation uses a drag law for spherical bodies on the whole trajectory. Fig. 9a shows the drag of a sphere as a function of the Reynolds number. Until impinging the ground, mass and diameter of the droplets will be reduced by evaporation (Fig. 9b).

For sprays consisting mainly of water, this effect can be considered by the formula

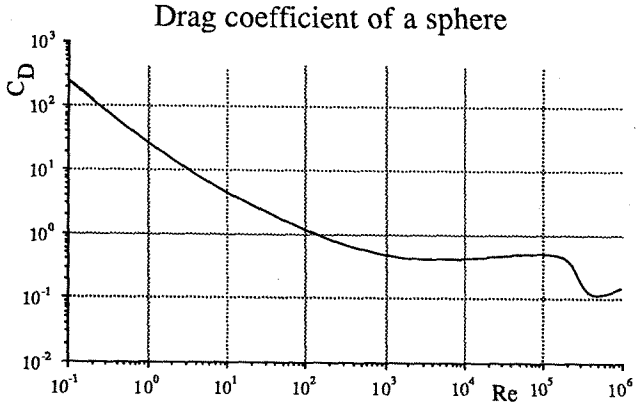


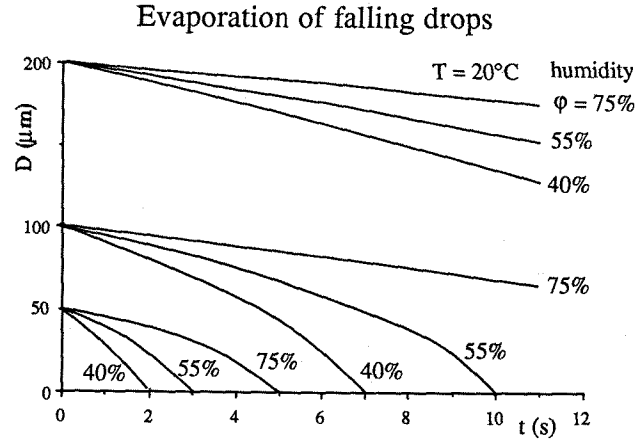


Figure 9. Drag and Evaporation of moving droplets

$$\frac{d}{dt}D^2(t) = -85 \cdot 10^{-12} \Delta T \left( 1 + 0.27\sqrt{Re} \right) \quad (7)$$

where D(t) is the droplet diameter and ΔT is the difference of the local temperature and the dewpoint temperature.

The velocity of the air flow is computed from the disturbance created by the propeller and the wake of the wing. To smooth the velocities induced by the vortex filaments, a Rankine vortex model is applied.

During the first 25 meters of the wake, the velocities are computed using the three-dimensional roll-up model. Then, a two-dimensional vortex model is used.

Droplet trajectories resulting from this computation do not take into account the influence of cross-wind and turbulence. Both effects are accounted for by additional models applied to the computed droplet impact point. The advantage of this method is the possibility to compute spray distributions for different cross-winds and levels of turbulence without the need of recomputing the droplet trajectories.

The computation of cross-wind drift is based on the assumption that droplets and wake are carried at the velocity of the wind so that mass forces can be neglected (Fig. 10). Then the drift is proportional to wind velocity and droplet flight time.

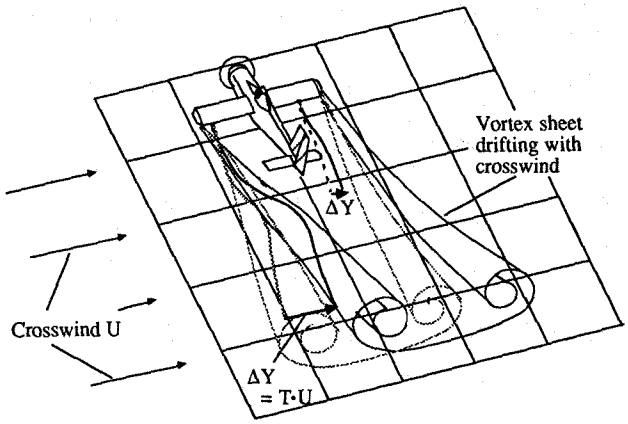


Figure 10. Principal influence of cross-wind on vortex sheet and spray

As the wind normally exhibits boundary layer effects at low altitudes, the variation in wind speed with height has to be considered. In the computation the following wind profile is used

$$U(h) = U_{fl} (h / H_{fl})^{0.16} \quad (8)$$

where $U_{fl}$ is the wind speed measured at the airplane's altitude.

The computation of the droplet motion involves an equivalent falling time $T_e$, defined by the integral

$$T_e = \int_0^T U(h) / U_{fl} \, dt \quad (9)$$

This value considers the change in cross-wind along the droplet trajectories. Hence, $T_e$ can be used to compute the cross-wind drift (Fig.11) for any given level of wind velocity $U_{fl}$ by

$$\Delta Y = U_{fl} \, T_e \sin(\varphi) \quad (10)$$

where

φ is the direction of wind

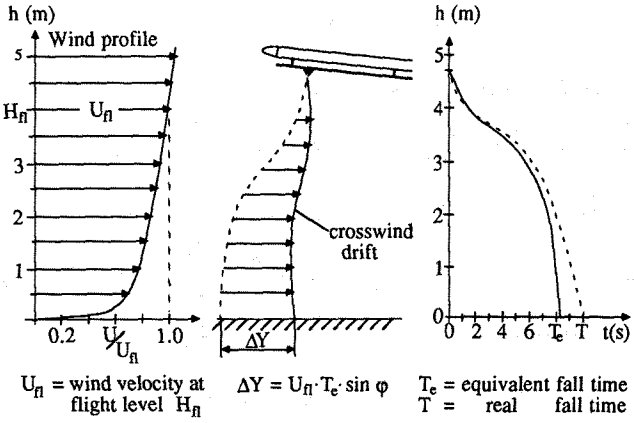


Figure 11. Influence of cross-wind profile on droplet drift

This procedure is based on the assumption that the vortex field is not distorted by the wind. This assumption is reasonable for low levels of cross-wind (U<2 m/s) as has been proved by computations using the point vortex method.

A spray cloud released under non-zero wind conditions will not only drift laterally but also will be diffused by the turbulence connected with the wind. The main influence of the turbulence is the prolongation of the flight time of the droplets resulting in a higher lateral drift under cross-wind conditions. Under normal weather conditions the intensity of turbulence i, defined as root mean square of the airspeed fluctuations normalized by the wind speed at flight level, can be assumed to be constant with time and height. Then, the root mean square of the velocity fluctuations is given as $\overline{u_T^2} = \overline{(i\,U_{fl})^2}$ where $u_T$ is approximately Gaussian distributed[18-20].

In turbulent air, the droplet is affected by the relative flow velocity

$$U_{rel} = U_{wake} + U_{wind} + u_T(t) - \dot{x} \qquad (11),$$

where

$u_T$ = velocity fluctuations due to turbulence.

If a simplified drag law

$$C_D = \text{const} / Re \qquad (12),$$

is used, Eq. (6) becomes linear and can be solved by superposition.

The simulation determines the trajectories of the droplets without considering turbulence by solving Eq. (6) in the form

$$\ddot{\vec{x}}_1 = \vec{g} + \beta\,(\vec{U}_{wake} - \dot{\vec{x}}_1)$$

with

$$\beta = 18\,\nu\,\rho / (\rho_D\,D^2)$$

where

$\rho$ and $\rho_D$ are the densities of air and droplets respectively.

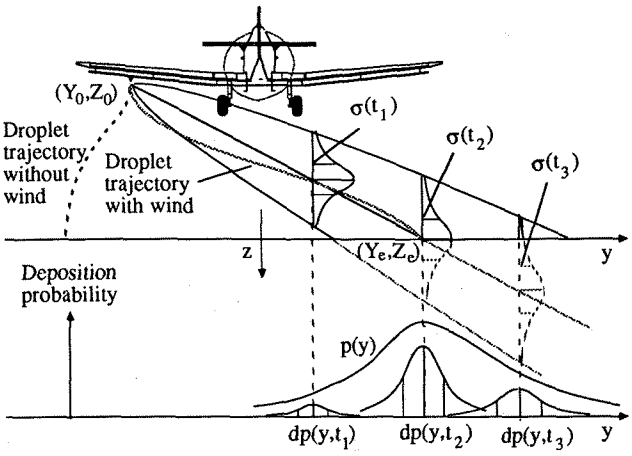


Figure 12. Spray deposition pattern with consideration of cross-wind and turbulence

The influence of cross-wind is included by the convection term

$$\ddot{\vec{x}}_2 = \beta\,\vec{U}_{wind}$$

The turbulence is considered by the equation for the third term

$$\ddot{\vec{x}}_3 = \beta\,(\vec{u}_T - \dot{\vec{x}}_3)$$

For the vertical component of $x_3$ (=z), the equation

$$\ddot{z} = -\beta\,(\dot{z} - u_{Tz}) \qquad (13)$$

has to be solved. Langevin[19] has investigated the stochastic characteristics of the term z and found, that the mean square value of z can be given as the following function of time

$$\sigma_z^2(t) = \overline{u_T^2}\,[\,2\,t/\beta - (2/\beta^2)\,\{1-\exp(-\beta\,t)\}]. \qquad (13)$$

Assuming that the random disturbances $u_T$ are independent of the direction, the mean square of the droplet dispersion is also independent of the direction

$$\sigma_x(t) = \sigma_y(t) = \sigma_z(t) = \sigma(t). \qquad (14)$$

For combining the turbulence model with the computed droplet trajectory and the cross-wind drift, it is assumed that the position of a droplet, which is not influenced by turbulence, is a linear function of time where starting position and deposition point are $(Y_0, Z_0)$ and $(Y_e, Z_e)$ respectively (Fig.16)

$$Y(t) = Y_0 + (Y_e - Y_0)\;(t\,/\,T_e)$$
$$Z(t) = Z_0 + (Z_e - Z_0)\;(t\,/\,T_e)$$

$Y_e$ contains the influence of cross-wind given in Eq. 10.

The probability density of the vertical dispersion of a droplet emitted by a nozzle can be written as

$$p(z, Z(t), t) = \frac{1}{\sqrt{2\pi}\;\sigma(t)} \exp\left(-\frac{(z - Z(t))^2}{2\,\sigma(t)^2}\right) \qquad (15)$$

Then, the probability that the droplet will be deposited until time t may be written as

$$\int_0^\infty p[z, Z(t), t]\,dz = ERF\left[Z(t)/\{\sqrt{2}\,\sigma(t)\}\right] = ERF\left[F(t)\right] \qquad (16)$$

The probability for touching the ground in the time intervall t...t+dt is given by (d ERF[F(t)]/dt) dt. Due to Eq. 14 the probability density for the distribution in lateral direction is as well Gaussian and given by

$$d\,p(y, t) = (d\,ERF[F(t)]\,/\,dt)\,\frac{1}{\sqrt{2\pi}\,\sigma(t)} \exp\left(-\frac{(y - Y(t))^2}{2\,\sigma(t)^2}\right) dt$$

In total, the distribution of the spray under the influence of wind and turbulence in lateral direction is found by integrating this equation from o to ∞. This operation can be easily per-

formed after discretization and numerical integration leading to the probability density p(y) of a single droplet describing the lateral dispersion due to turbulence and cross-wind.

## VI. Simulation of Spray Distribution

Up to this point only the deposition of single droplets has been considered. To simulate a ground deposition pattern, as found in experiments, a statistical evaluation of the droplet characteristics has to be incorporated in the simulation. The droplets ejected by spray nozzles and found after the break-up phase differ in size and flow direction. Therefore, further information, which must be modeled on the basis of experiments, is required.

The simulation of the spray nozzle characteristics must account for

- the flow directions of the droplets,
- the spectrum of the droplet diameter and
- the velocity range of the droplets.

Fig. 13 shows the model used for the simulation. The droplets are assumed to be ejected along a cone, on which a number of droplets are emitted. The cone is defined by two opening angles (kx, ky) and the direction of the cone axis (kz).

The initial velocity of the droplets is computed using the known spray duct pressure

$$V_{Do} = \sqrt{((P_{duct} - P_{air})\,(2/\rho)\,K)}$$

With the assumption that 50% of the difference pressure is converted into droplet velocity K = 0.5. The droplet size spectrum found in experiments (Fig. 14) can be approximated by a Gaussian distribution (on a logarithmic scale). For the computation the spectrum is discretized. As the droplet size has an essential effect on the droplet trajectories, the simulation uses n=7 different droplet classes (Fig. 14).

In a large data base droplet trajectories have been collected , which are sufficient to compute spray distributions for a number of parameters. These include

-windspeed
-spray duct pressure
-spray cone angle
-droplet diameter spectrum
-nozzle numbers and position and
-intensity of turbulence.

The simulation evaluates the spray deposition pattern with respect to the fraction of area wetted by spray.

The spray distribution for a single nozzle is composed of the contribution of a number of droplets (total number $N_D$). Because the relative frequency $f_j$ and the volume $V_{Dj}$ of droplets in any class j is given, the total number of droplets $N_D$, emitted by a nozzle with a spray flux of Q, is given by

$$N_D = \frac{Q}{\sum_{j=1}^{n} f_j V_{Dj}}$$

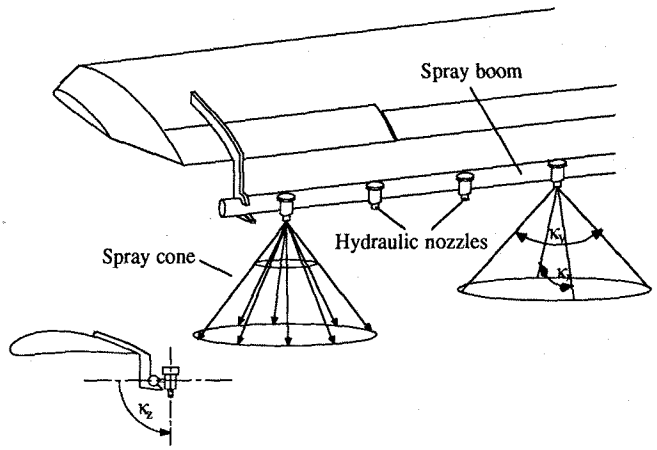


Figure 13. Simulation of spray nozzle characteristics

In the simulation m droplets trajectories (index k) in each of n classes have been calculated. Corrresponding to the relative frequency $f_j$, the expectation value of droplets deposited in the range y to y+dy is given by

$$\sum_{j=1}^{n} f_j \sum_{k=1}^{m} p_{jk}(y)\,dy$$

In this term, $p_{jk}(y)$ is the probability density introduced above. Then, the area wetted by these droplets becomes

$$\sum_{j=1}^{n} f_j \sum_{k=1}^{m} p_{jk}(y)\,A_{jk}\,dy \qquad (17)$$

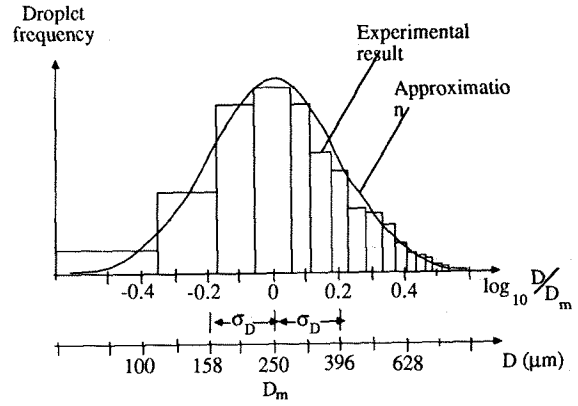


| Droplet class j | 1 | 2 | 3 | 4 | 5 | 6 | 7 |
|---|---|---|---|---|---|---|---|
| Mean drop size $D_j$(µm) | 125 | 175 | 225 | 275 | 350 | 450 | 550 |
| Relative droplet frequency $f_j$ | 0.110 | 0.180 | 0.186 | 0.153 | 0.192 | 0.087 | 0.043 |

Figure 14. Droplet classes used in the simulation

where the droplet (j,k) covers an area $A_{jk}$ which depends on the droplet size at the time of impact considering the evaporation effect. The number of droplets and the area defined by Eq. (17) have to be scaled by $(N_D/m)$ leading to a totel wetted area $A_w$ depending on y. Finally, the fraction of area wetted by spray is given by

$$a_w(y) = \frac{A_w(y)}{V\,dy} = \frac{N_D}{m\,V} \sum_{j=1}^{n} f_j \sum_{k=1}^{m} p_{jk}(y)\, A_{jk}$$

Fig 20. compares the spray distributions of a single nozzle for different directions (0°, 90°). In the diagramm is demonstrated that the statistical accuray is limited if turbulence is neglected

After computing the spray deposition patterns for any spray nozzle the total spray distribution for the aircraft can be determined. This final step requires only the superposition of the distributions for any nozzle defined on the boom.

## VII. Results of the Simulation

### Basic effects

The results shown in figure 16, obtained from the simulation, illustrate the following basic influences on droplet motion.

The tip vortices have an essential influence on the droplet motion near the wing tip. The ground effect increases the outward drift of the droplets as well as the flight time where both factors result in a higher sensitivity to crosswind.
As the flight time depends strongly on the droplet size, smaller droplets are more disturbed by the tip vortices than larger ones. This effect is magnified under crosswind conditions.

Propeller swirl is another important factor influencing the motion of the spray. The strong vortex shed from the left side of the wing (Fig. 3 and 6) and also the propeller slipstream create an inhomogeneous velocity field that leads to an unsymmetric spray distribution as can be seen from comparing right and left part of Fig. 16 b, c.

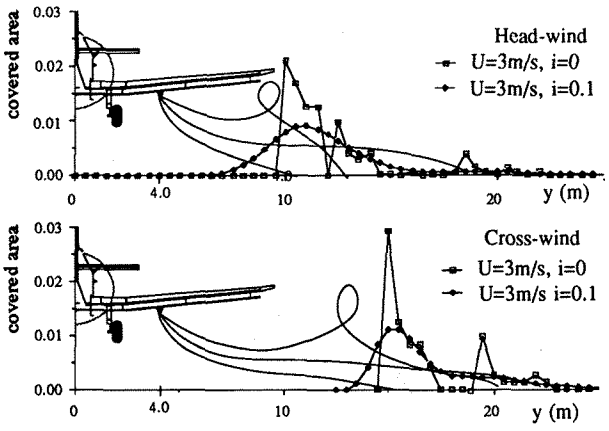


Figure 15. Spray deposition pattern for a single nozzle

During the flight tests in Nyiregyhza (Hungary) in October 1987, spray distributions of the PZL M-18 DROMADER have been evaluated. The weather conditions during these tests were not ideal, because the mean wind speed was quite high (about 3 m/s) and the turbulence level i amounted to values of 0.05...0.2. Furthermore, the direction of the wind was unsteady. Consequently, the wake of the wing often was blown over the wind measuring instrumentation therby causing disturbances on the recorded data.

Ground deposits were collected on film sheets and processed by a "Vidimet" picture processing unit. The sheets contained too many droplets to be counted individually. Therefore the fraction of area covered by droplets was evaluated to measure the spray distribution.

The flight test results were compared with simulation results. The data used for the simulation were:

- Droplet size range from 120(μm) to 550(μm) as shown in Fig. 14,
- Pressure inside the spray duct of 3.5 (bar), giving 15.8 m/s as droplet initial velocity,
- Flat-cone spray nozzles (Hungarian type szilper-1), represented by 11 droplets emitted on the cone for any of the 7 droplet classes (Fig.14). The spray cone is described by opening angles of ky=120 (degrees) and kx= 45 (degrees) respectively, while the spray direction is given by kz= 90 (degrees) (Fig. 13).

- Data for 101 equally spaced nozzles on the boom were computed to cover any possible spray nozzle arrangement.

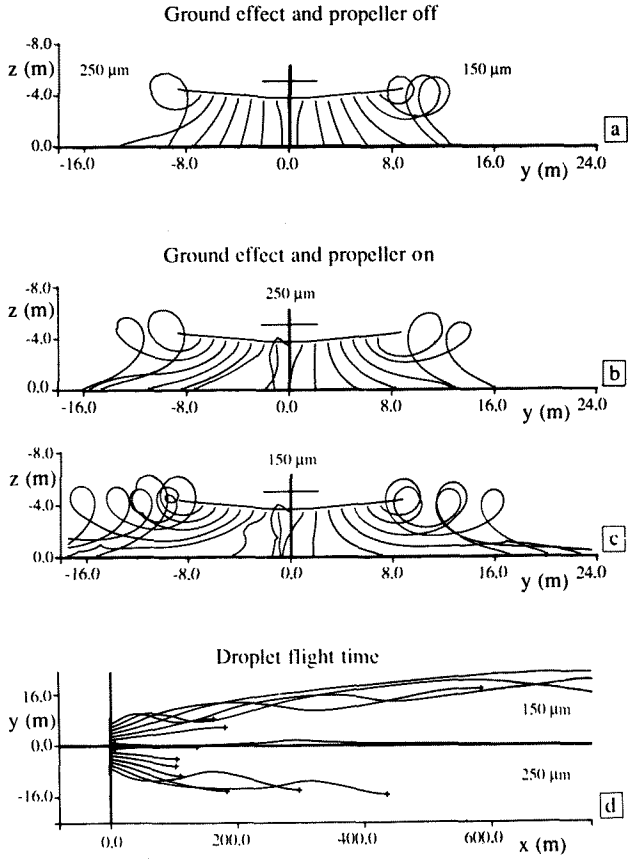


Figure 16. Droplet trajectories influenced by ground effect and propeller slipstream

The total numbers of droplet trajectories computed per spray nozzle was 77 resulting in 7777 trajectories for the spray boom. The computation time required for this computation was 33hrs on a Cyber 175.

- The ground distribution was evaluated in intervals of $\Delta Y = 1$ m which matches the resolution of the experiments.

- The spray flux Q per nozzle was set to the measured value of 0.116 (l/s).

Fig. 17 compares simulation results with the distribution obtained from a flight using the standard nozzle arrangement of the Hungarian Agricultural Flight Service. The agreement between flight tests and simulation is satisfactory, although the influence of the propeller, evaluated in the simulation, is too strong. The spray width as well as the mean value of the spray deposition are well correlated.

In the standard procedure, used by the Hungarian Agricultural Flight Service to determine the uniformity of the spraying, several spray flights are performed in opposite directions and the corresponding spray distributions are superimposed. Since the experimental data were recorded only for one flight direction and, thus, for one crosswind direction, the spray distributions for the opposite flight direction had to be estimated. In the simulation the correct distributions found for the opposite wind direction were superimposed. The root mean square value of the variation in the fraction of wetted area, $a_w$, called CV,

$$CV^2 = \frac{\overline{(a_w(y) - \bar{a}_w)^2}^y}{\bar{a}_w^2}$$

was evaluated as a measure of uniformity. Values of CV<0.3 are considered as acceptable and define the maximum widths of spray corridors. In Figure 18, CV is shown for experiments and simulations covering three wind conditions. The comparison shows good agreement. The maximum usable corridor width is determined by an extrapolation using the slope of the outer parts of the curves. The values resulting for CV=0.3 are 23m for both simulations and experiments.

The difference in experimental and simulation result are caused by two effects which could occur because the computations preceeded the flight tests. The power rating used in the simulation was too high and the lift distribution was computed for the maximum take-off weight, while the flight tests were performed with minimum weight and 50% power setting. Although the figures shown in the previous sections already are adapted to the experimental values, but the mass of droplet trajectories could not be recomputed up to now.

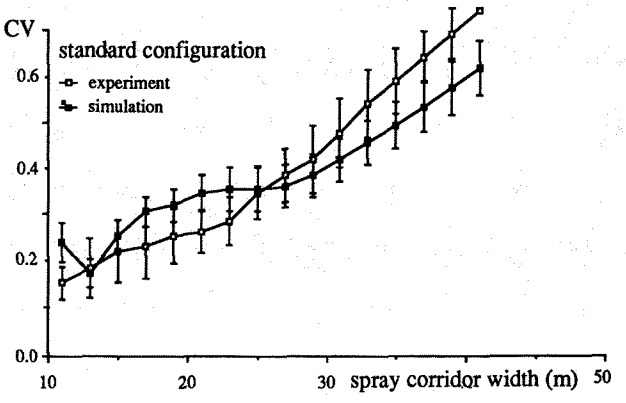


Figure 18. Comparison of the statistical parameter CV obtained from experiments and simulations

## VIII. Methods for Improving Spraying Efficiency

The spray distributions, produced by the DROMADER in standard configuration, can be improved by modifications. The modifications investigated here are shown on the right hand side of Fig. 19 and consider the installation of winglets, the optimization of spray nozzle arrangement and spray boom position.

The development of a winglet for the DROMADER had to consider the load limitations of the wing as well as the increase in rolling-moment due to sideslip accepted by the pilots.

The optimization of the winglet geometry is done by a computer program using a lifting line theory. Input is the configuration of original wing, an estimation for the winglet shape and

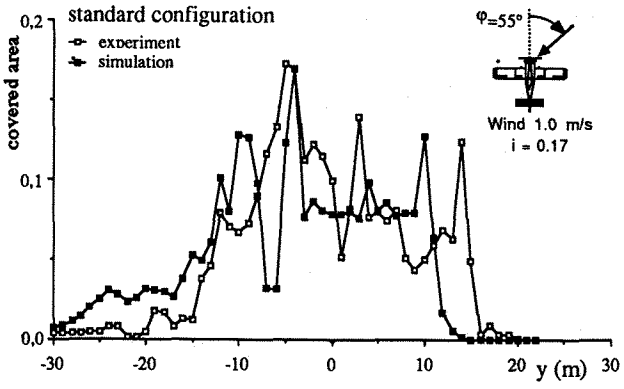


Figure 17. Spray distribution for DROMADER in standard configuration

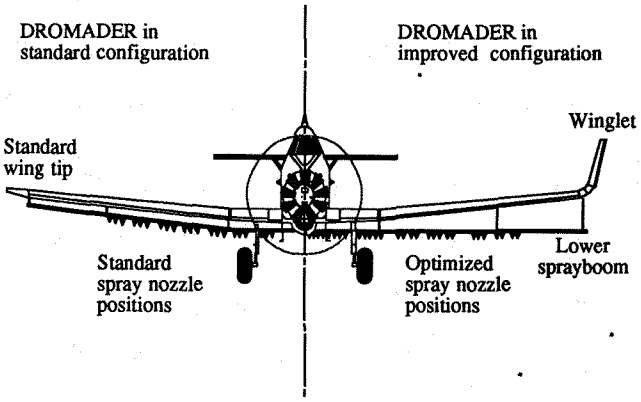


Figure 19. Improved configurations investigated for DROMADER

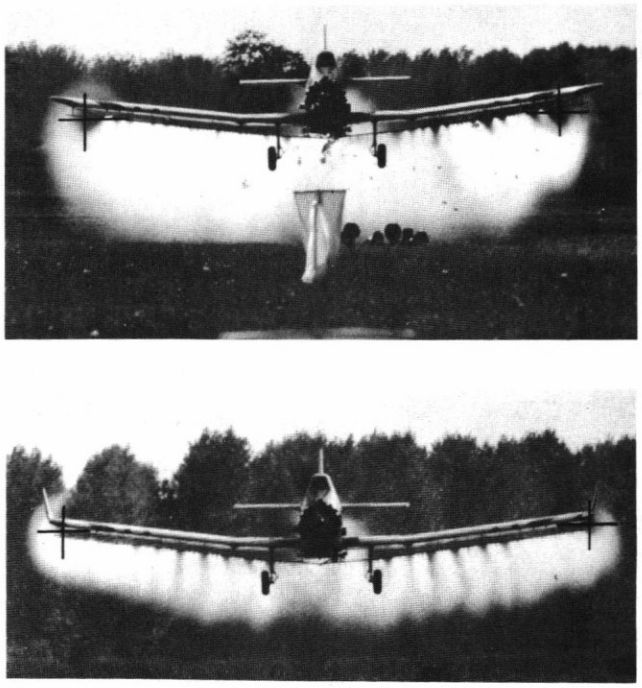

Figure 20. Tip vortex displacement achieved by winglets

the maximum wing root bending moment. For this configuration the chord distribution (Fig. 7a) on the winglet is optimized for minimum induced drag.

The winglet design uses a large angle of incidence on the winglet itself. This ensures a reduced drag during maneuvers (high value of $C_L$) and a high load on the winglet during cruise. The latter effect shifts the tip vortices to a higher position.

Fig. 20 shows a photograph of the roll-up process. In the winglet case, the vortex cores are shifted 0.5 m outwards and 0.3 m above the position in the standard configuration. The corresponding results of the computation are $\Delta z = 0.44$ m and $\Delta y = 0.23$ m.

Winglets reduce the induced drag by 5.8% in cruise ($C_L = 0.55$) and 6.4% during climb ($C_L = 1.0$). The possible fuel saving is about 3% where 50% are saved during climbs and maneuvers.

Looking at the trajectories of single droplets (Fig. 21), the reduced tip vortex strength (-3.7% for the winglet case) and the favorable tip vortex position result in a smaller droplet drift so that the usable length of the spray boom could be raised from 10 meters (standard wing) to 12 meters (winglet). Nozzles spraying droplets of 150 (µm) can be used along a spray boom of 8 meters (6 meters without winglets). Fig. 28 shows the drift for 250 and 150 (µm) droplets respectively for a cross-wind of 2 m/s. The comparison between the two configurations demonstrates the advantages of the winglet.

Fig. 23 shows an example for the spray distributions achieved with winglets which again is in acceptable agreement with flight test.

It seemed reasonable to combine the advantages of winglets with a lower spray boom position The combination of both result in a considerable improvement of the spray deposition

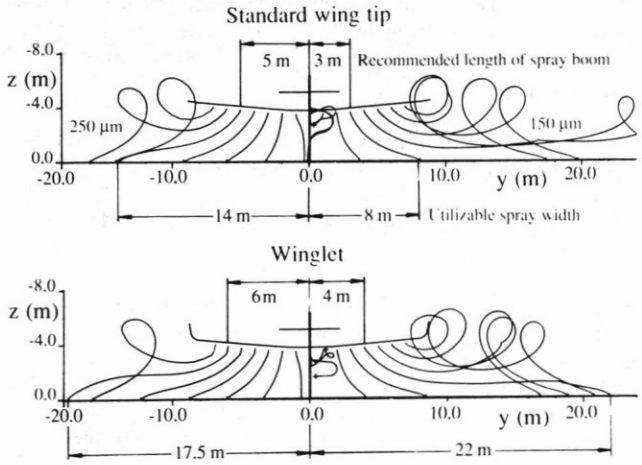


Figure 21. Effects of winglet on droplet trajectories

quality.

An important result of the simulation show that the spray nozzle arrangement must be optimized for any wing configuration. To demonstrate the spray quality, which could be achieved with the Dromader, an optimal nozzle arrangements for each wing configuration was determined in simulation and investigated in the flight tests.

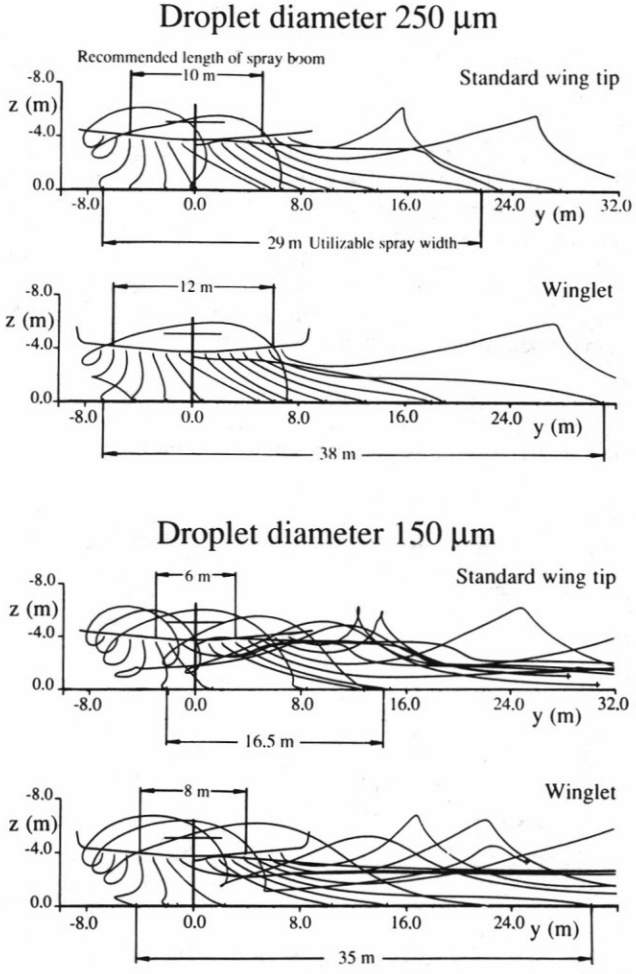


Figure 22. Reduction of cross-wind drifts by winglet

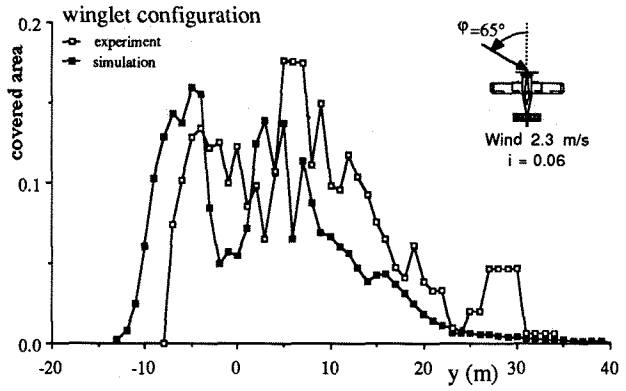


Figure 23. Comparison of spray distributions with winglets

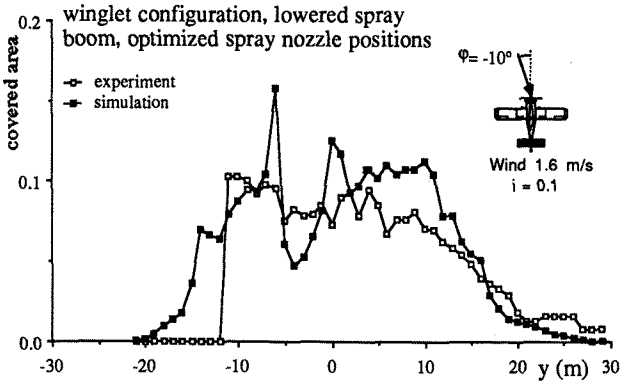


Figure 24. Spray distributions for DROMADER fitted with winglets and optimized spray nozzle installation

The optimization method used here is an evolution algorithm that switches randomly some spray nozzles on or off and evaluates the effects on the value of CV.

The spray distribution computed and measured for a configuration with winglets and lower spray boom position is shown in Fig. 24. In Fig. 25 the comparison of the statistical parameter CV is given. The results show a significantly improved uniformity compared to the results presented above.

The advantage in spray width achieved by the improved configuration could also be used for spraying smaller droplets. The results of the simulation indicate that a droplet diameter of 150 (μm) could give the same spray width as the standard configuration spraying 250 (μm) droplets. As the flight tests were limited to a fixed spray nozzle type there are no experimental data yet to prove these results.

## IX. Concluding Remarks

A numerical simulation is presented which is capable of predicting spray deposition patterns for agricultural aircraft configurations. It gives certain improvements over existing programms and promises higher accuracies in the calculated spraying distribution. In particular, new methods for describ-

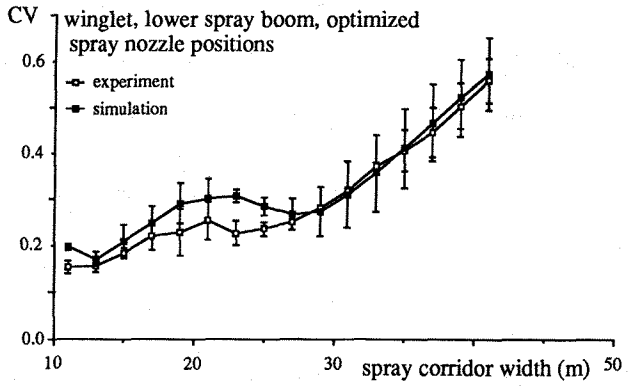


Figure 25. Comparison of uniformity of spray given bei CV

ing the roll-up process of the wing wake and the flow characteristics of the propeller slipstream were introduced. In addition, the statistical method for describing the influence of wind fields and turbulence has been refined.

Using this simulation program and an evolutionary optimization method, improvements in spray efficiency for various modifications of an existing aircraft have been developed. For a winglet configuration the spray efficiency could be considerably improved (by about 35%), if the spray nozzle arrangements were simultaneously optimized. The optimized configuration has been investigated in flight tests. The cooperation with the Technical University of Budapest enabled to perform these tests in Hungary using an agricultural airplane of PZL M-18 DROMADER type. In general, a good agreement between flight tests and simulation results was found.

The obtained improvements can be of benefit in two aspects. First, an enlargement of the width of spray corridors is possible, which will decrease the time to treat the agricultural area. Secondly, the droplet sizes can be reduced which would lower the costs for chemicals as well as the environmental pollution.

## Acknowledgments

The authors wish to thank the Deutsche Forschungsgemeinschaft (DFG) for the financial support of this research.

## References

1. Schaefer, G. W., "The role of aircraft in an agricultural strategy for the year 2000", Aeronautical Journal, June 1980

2. Bals, E. J., "The importance of controlled droplet application (CDA) in pesticide applications", Proceedings 8th British Insecticide and Fungicide Conference, (1975)

3. Bals, E. J., "The reasons for the development of the controlled droplet application (C.D.A.),concept and thoughts on the application and its pinciples", Med. Fac. Landbouww. Rijksuniv., Gent, 41/2, 1976

4. Johnstone, D. R., "Statistical description of spray drop size for controlled drop application", Symposium on Controlled

Drop Applications, April 1978

5. Johnstone, D. R., "The influence of physical and meteorological factors on the deposition and drift of spray droplets of controlled size", Symposium on Controlled Drop Applicaions, April 1978

6. Reed, W. H., "An Analytical Study of the Effect of Airplane Wakes and the Lateral Dispersion of Areial Sprays", NACA TN 1196, 1954

7. Reed, W. H., "An Analytical Study of the Effect of Airplane Wake on the Lateral Dispersion of Aerial Sprays", NACA TN 3032

8. Trayford, R. S., L. W. Welch, "Agricultural Aviation Research, 3. The Simulation of Aerial Spray Trajectories", Commonwealth Scientific and Industrial Research Organization (CSIRO), Division of Mechanical Engineering, Internal Report No 110, Melbourne, Sept. 1972

9. Trayford, R. S., Welch, L. W., "Aerial Spraying: A Simulation of Factors Influencing the Distribution and Recovery of Liquid Drops", J. agric. Engng., Res. (1977) 22, pp 183-196

10. Miranda, L. R., Elliott, R. D., Baker, W. M., "A Generalized Vortex Lattice Method for Subsonic and Supersonic Flow Applications", NASA Contractor Report 2865 (1977)

11. Müller, R. H. G., "The Influence of Winglets on Rotor Aerodynamics", Vertica (1987), Vol 11, No 4, pp 601-618

12. Schröder, W., "Berechnung der nichtlinearen Beiwerte von Flügeln mit kleinem und mittlerem Seitenverhältnis nach dem Wirbelleiterverfahren in inkompressibler Strömung", Forschungsbericht der DFVLR (1978), DFVLR-FB 78-26

13. Routh, E. J., Proceedings of the London Mathematical Society, 12, (1881), pp.73-89

14. Staufenbiel, R., "Structure of Lift-Generated Rolled up Vortices", Journal of Aircraft, vol 21, No 10, Oct 1984, pp 737-744

15. Staufenbiel, R., "Ein Modell zur analytischen Beschreibung von Randwirbeln", ZFW.9 (1985), Vol.5

16. Betz, A., "Verhalten von Wirbelsystemen", Z. angew. Math. Mech. 12 (1932), pp.164-174

17. Verstynen, H. A., Dunham, R. E."A flight investigation of the trailing vortices generated by ajumbo jet transport", NASA TN D-7172, April 1973

18. Ciffone, D. L., Orloff, K. L., "Far Field Wake-Vortex Characteristics of Wings", Journal of Aircraft, vol.12, May 1975, pp.464-470

19. Bach, D. H., Sayer, W. J. D., "Transport of Aerial Spray, I. A Model of Aerial dispersion", Agricultural Meteorology, 15(1975) pp.257-271

20. Pasquill, F., "Atmospheric Diffusion", Publisher Ellis Horwood, UK, 2nd Edition, pp 429, 1974

21. Hay, J. S., Pasquill, F., "Diffusion from a continuous source in relation to the spectrum and scale of turbulence", In: Frenkiel, F. N. and Shepherd, P. A. (Editors), Atmospheric Diffusion and Air pollution, Acad. Press, Adv.Geophys., 6:345-365 (1959)